Accepted Manuscript

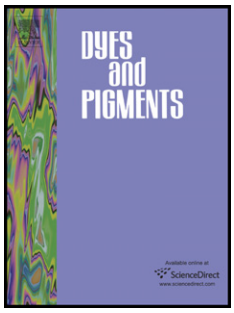

Rhodamine-pyrene conjugate chemosensors for ratiometric detection ofHg2+ions: Different sensing behaviorsbetween aspirolactone and aspirothiolactone

Kai-Hui Chu, Yi Zhou, Yuan Fang, Li-Hong Wang, Ju-Ying Li, Cheng Yao

PII: S0143-7208(13)00069-7

DOI: 10.1016/j.dyepig.2013.02.019

Reference: DYPI 3866

To appear in: *Dyes and Pigments*

Received Date: 19 December 2012

Revised Date: 26 February 2013

Accepted Date: 26 February 2013

Please cite this article as: Chu K-H, Zhou Y, Fang Y, Wang L-H, Li J-Y, Yao C, Rhodamine-pyrene conjugate chemosensors for ratiometric detection ofHg2+ions: Different sensing behaviorsbetween aspirolactone and aspirothiolactone, *Dyes and Pigments* (2013), doi: 10.1016/j.dyepig.2013.02.019.

Graphical Abstract.tif

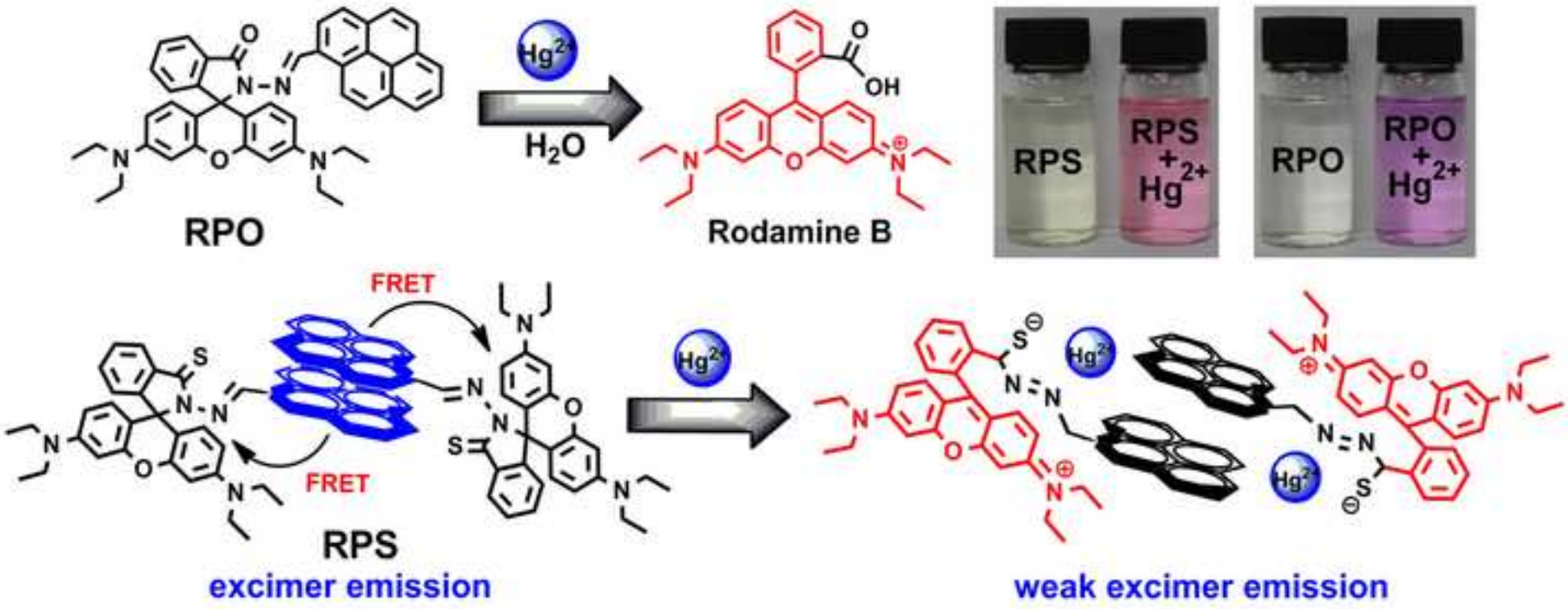

Rhodamine-pyrene conjugate chemosensors for ratiometric detection of Hg^{2+} ions: Different sensing behaviors between a spirolactone and a spirothiolactone

Kai-Hui Chu, Yi Zhou*, Yuan Fang, Li-Hong Wang, Ju-Ying Li, Cheng Yao*

State Key Laboratory of Materials-Oriented Chemical Engineering and College of Science, Nanjing University of Technology, Nanjing 211816, P. R. China

*Corresponding author. Tel: +86-25-5813-9482; Fax: +86-25-5813-9482

E-mail: yaochengnjut@126.com (C. Yao); zhouyi624@126.com (Y. Zhou)

Abstract

Two novel rhodamine-pyrene conjugated chemosensors were successfully designed and synthesized, which exhibited high affinity to Hg^{2+} ions. As ratiometric chemosensors, each displayed highly selective and sensitive colorimetric and fluorogenic dual-responses towards Hg^{2+}. The comparison of two chemosensors indicated that the spirothiolactone containing sensor was superior to the spirolactone analogue in sensing behavior when detecting Hg^{2+}, presumably due to the thiophilic nature of mercury and the different sensing mechanisms in operation. Upon interaction with Hg^{2+}, the spirothiolactone showed a 1:1 stoichiometry for the Hg^{2+} complex, accompanied with a weakened fluorescence resonance energy transfer (FRET) behavior. However, the spirolactone was hydrolyzed and consequently induced the monomer-exciemer switch of the resulted pyrene in the presence of Hg^{2+} ions.

Key words: rhodamine; pyrene; mercury; fluorescent chemosensors; FRET; excimer emission

1. Introduction

As we know, in the environment, mercury pollution can be caused by natural phenomena and human activities, including volcanic eruptions, wind erosion, water erosion, solid waste incineration and industrial production [1]. Mercury can gain access to the body orally or dermally, and inorganic mercury can be converted by bacteria into methyl mercury in the environment, which subsequently bioaccumulates through the food chain. As one of the most highly toxic and hazardous contaminants, once absorbed in the human body, even at very low concentrations, mercury can cause serious human health problems, which results in permanent damages to the brain, nervous system, DNA, mitosis, kidneys, and endocrine system [2]. Accordingly, the effective and selective detection of mercury for biochemistry, environmental science and medicine, is highly desirable and indispensable [3].

Compared with conventional analyzing/detecting methods of Hg^{2+}, such as atomic absorption and emission spectroscopy, inductively coupled plasma mass spectrometry, selective cold vapor atomic fluorescence spectrometry, neutron activation analysis, electrochemical sensoring, X-ray microanalysis and a variety of potentiometric ion-selective electrodes, *etc.*, analytical techniques based on UV-vis and fluorescence spectroscopy are very popular in terms of nondestructive, rapid, highly selective and sensitive detection. As a result, developing new practical and optical chemical sensors (optodes) that exhibit dual-responsive chromogenic and fluorogenic detection of Hg^{2+} ions is still a challenge [4].

Rhodamine-based dyes are widely used for their excellent spectroscopic properties, such as large absorption coefficient, high fluorescence quantum yield, absorption and emission at a long wavelength [5]. Generally, in the presence of specific metal ions, the colorless and nonfluorescent rhodamine spirolactam structure would be converted into the colored and highly fluorescent ring-opened amide form, which provides not only excellent enhancement in absorption and fluorescence intensity, but also direct visual detection [6]. Moreover, the long emission wavelength (> 550 nm) can often be preferred to serve as reporting groups for analytes to avoid the influence of background fluorescence (< 500 nm) [7]. Recently, many rhodamine-based chromogenic and fluorogenic chemosensors have been extensively applied to selectively sense heavy metal ions, such as Hg^{2+} ions, with an “off-on” mechanism [8]. On the other hand, the pyrene moiety is one of the most useful fluorophores in the construction of fluorogenic chemosensors for a variety of important

chemical species [9]. Pyrene is widely employed as ratiometric fluorescent chemosensors, due to its well-known photophysical properties in monomer/excimer emission switching [10].

Yoon et al. reported a rhodamine-pyrene sensor which was designed as a ratiometric and "off-on" sensor for the detection of Cu^{2+} [11]. Subsequently, Kim et al. developed a Hg^{2+}-selective probe with a calix[4]arene scaffold appended rhodamine and pyrene moiety [12]. Herein, considering the optical and configurable characteristics of rhodamine and pyrene subunits, we design novel ratiometric chromogenic and fluorogenic chemosensors **RPS** (spirothiolactone) and **RPO** (spirolactone) (Scheme 1) for sensitive, selective and reversible detection of Hg^{2+} in aqueous medium, introducing a pyrene moiety into the rhodamine fluorophore. The two chemosensors are structurally similar, but they show different sensing mechanisms upon the interaction with Hg^{2+}.

<Place Scheme 1 here.>

2. Experimental

2.1 Apparatus and reagents

UV-visible spectra and fluorescence spectra were recorded on a Perkin-Elmer 35 spectrometer and a Perkin-Elmer LS 50B fluorescence spectrophotometer at room temperature, respectively. ^{1}H-NMR and ^{13}C-NMR were measured on a BrukerAV-500 or BrukerAV-300 spectrometer with chemical shifts reported in ppm (in $CDCl_3$; TMS as internal standard). Electrospray ionization mass spectra (*ESI*-MS) were measured on a Micromass LCTTM system. All pH measurements were made with a Sartorius basic pH-Meter PB-10. Melting points were determined on a hot-plate melting point apparatus XT4-100A and were uncorrected. Chromatographic separations were done by column chromatography using 200-300 mesh silicagel.

Unless otherwise noted, materials were obtained from commercial suppliers and were used as received. All the solvents were of analytic grade. Water was re-distilled. The salts used in stock solutions of metal ions were $NaNO_3$, KNO_3, $Mg(NO_3)_2{\cdot}6H_2O$, $Ca(NO_3)_2{\cdot}4H_2O$, $FeCl_2{\cdot}4H_2O$, $MnCl_2{\cdot}4H_2O$, $Ni(NO_3)_2{\cdot}6H_2O$, $Co(NO_3)_2{\cdot}6H_2O$, $Cu(NO_3)_2{\cdot}3H_2O$, $Zn(NO_3)_2{\cdot}6H_2O$, $Cd(NO_3)_2{\cdot}4H_2O$, $AgNO_3$, $Hg(ClO_4)_2{\cdot}3H_2O$, $Pb(NO_3)_2$ and $CrCl_3{\cdot}6H_2O$. Rhodamine B and 1-pyrenecarboxaldehyde were purchased from Alfa Aesar. The other reagents were purchased from Taiyuan RHF Reagents Ltd.

2.2 General procedures of spectra detection

Stock solutions (10^{-2} M) of the nitrate salts (or chlorate salts) of Na^{+}, K^{+}, Mg^{2+}, Ca^{2+}, Fe^{2+}, Mn^{2+},

Ni^{2+}, Co^{2+}, Cu^{2+}, Zn^{2+}, Cd^{2+}, Ag^{+}, Hg^{2+}, Pb^{2+} and Cr^{3+} in water were prepared. Stock solutions (1.0×10^{-4} M) of **RPS** and **RPO** were prepared in ethanol. Before spectroscopic measurements, the solution of **RPS** and **RPO** was freshly prepared by diluting the high concentration stock solution to corresponding solution. All the measurements were made according to the following procedure. To 10 mL glass tubes containing different amounts of metal ions, appropriate amounts of solution of chemosensors **RPS** or **RPO** were added directly by pipette, then diluted with ethanol and deionized water to 10 mL ($EtOH/H_2O$ = 1:1, v/v) and mixed, then the absorption and fluorescence sensing of metal ions were run. In selectivity experiments, the test samples were prepared by placing the appropriate amounts of metal ions stock solution into 10 mL solution of **RPS** (3 μM) or **RPO** (5 μM). All samples containing **RPS** and **RPO** were prepared at room temperature and shaken for 10 s. Then waited for 5 min and 80 min respectively before UV-vis and fluorescence spectra measurements. Excitation wavelength was 365 nm for **RPS**, 365 nm and 515 nm for **RPO**.

The wide pH range solutions were prepared by adjustment of HCl or NaOH solutions.

2.3 Synthesis

*2.3.1 Synthesis of Rhodamine-B hydrazide **4***

Rhodamine B hydrazide was synthesized according to the reported method [13]. ^{1}H-NMR (500 MHz, $CDCl_3$): δ = 7.93 (d, J = 5.4 Hz, 1H, Ar-H), 7.44 (d, J = 3.6 Hz, 1H, Ar-H), 7.42 (d, J = 3.6 Hz, 1H, Ar-H), 7.10 (d, J = 5.6 Hz, 1H, Ar-H), 6.46 (d, J = 8.0 Hz, 2H, Xanthene-H), 6.42(d, J = 3.2 Hz, 2H, Xanthene-H), 6.29 (m, 2H, Xanthene-H), 3.60 (s, 2H, $-NH_2$), 3.34 (q, J = 7.0 Hz, 8H, $-CH_2-$), 1.16 (t, J = 7.0 Hz, 12H, $-CH_3$).

*2.3.2 Synthesis of Thiooxorhodamine-B hydrazide **3***

Rhodamine B hydrazide (5.0 mmol, 2.28 g) and Lawesson's Reagent (5.0 mmol, 2.03 g) were dissolved in dry toluene (60 mL), and the reaction mixture was refluxed at 85°C for 24 h under N_2 atmosphere and evaporated under reduced pressure. The residue was added to K_2CO_3 saturated solution and stirred for 2 h at room temperature, and then extracted by CH_2Cl_2. After removal of CH_2Cl_2, the residue was purified by flash chromatography (CH_2Cl_2 / petroleum, 4:1, R_f = 0.4) as eluent to afford Thiooxorhodamine B hydrazide (0.87 g, yield: 37%). M.p. 185.4~186.7 °C. R_f = 0.4 (SiO_2; CH_2Cl_2 / petroleum, 4:1). ^{1}H-NMR (500 MHz, $CDCl_3$): δ = 8.09 (d, J = 7.2 Hz, 1H, Ar-H), 7.46 (m, 2H, Ar-H), 7.10 (d, J = 7.2Hz, 1H, Ar-H), 6.43 (s, 2H, xanthene-H), 6.35 (d, J = 8.8Hz, 2H, xanthene-H), 6.27 (m, 2H, xanthene-H), 4.81 (s, 2H, $-NH_2$), 3.34 (q, J = 7.0Hz, 8H, $-CH_2-$), 1.16 (t, J

= 7.0Hz, 12H, -CH_3). ^{13}C-NMR (75 MHz, $CDCl_3$): 182.93, 153.45, 149.26, 149.20, 136.36, 131.95, 128.50, 128.02, 124.53, 123.05, 108.02, 103.34, 97.98, 44.34, 12.55. Anal. Calcd for $C_{28}H_{32}N_4OS$: C, 71.15; H, 6.82; N, 11.85. Found: C, 71.24; H, 6.86; N, 11.77. TOF-MS: m/z 473.16 $[M+H]^+$.

*2.3.3 Synthesis of chemosensor **2** (**RPO**)*

Rhodamine B hydrazide **4** (1.0 mmol, 0.46 g) and 1-Pyrenecarboxaldehyde (1.0 mmol, 0.23 g) were dissolved in anhydrous boiling methanol (20 mL), the reaction mixture was refluxed at 65 °C for 12 h under N_2 atmosphere. The resulting yellow precipitate was filtered and washed with cold methanol to afford a yellowish solid of **RPO** (0.42 g, yield: 63%). M.p. 192.1~192.7 °C. ^{1}H-NMR (300 MHz, $CDCl_3$): δ = 9.64 (s, 1H, imine-H), 8.45-8.47 (d, J = 8.1, 1H, Ar-H), 8.15-8.18 (d, J = 9.3, 1H, Ar-H), 8.07-8.09 (d, J = 7.5, 3H, Ar-H), 7.99-8.02 (d, J = 8.1, 1H, Ar-H), 7.89-7.96 (m, 4H, Ar-H), 7.48-7.58 (m, 2H, Ar-H), 7.19-7.21 (d, J = 7.2, 1H, Ar-H), 6.63-6.66 (d, J = 9, 2H, Ar-H), 6.56 (s, 2H, Ar-H), 6.26-6.29 (d, J = 8.7, 2H, Ar-H), 3.31 (q, J = 6.6, 8H, -CH_2-), 1.12 (t, J = 6.9, 12H, -CH_3). ^{13}C-NMR (300 MHz, $CDCl_3$): 165.00, 153.21, 151.85, 148.98, 145.54, 133.36, 132.05, 131.18, 130.55, 129.52, 129.30, 128.33, 128.23, 128.04, 127.90, 127.37, 125.81, 125.42, 125.10, 125.04, 124.78, 124.58, 124.48, 123.92, 123.38, 122.79, 108.22, 106.09, 97.96, 66.11, 44.32, 12.57. Anal. Calcd for $C_{45}H_{40}N_4O_2$: C, 80.81; H, 6.03; N, 8.38. Found: C, 80.89; H, 6.08; N, 8.31. TOF-MS: m/z 669.2 $[M+H]^+$.

*2.3.4 Synthesis of chemosensor **1** (**RPS**)*

The synthesis of chemosensor **RPS** is similar to that of chemosensor **RPO**. Thiooxorhodamine B hydrazide (1.0 mmol, 0.47 g) and 1-Pyrenecarboxaldehyde (1.0 mmol, 0.23 g) were dissolved in anhydrous boiling methanol (20 mL), and the reaction mixture was refluxed at 65 °C for 12 h under N_2 atmosphere. The resulted yellow precipitate was filtered and washed with cold methanol to afford a yellowish solid of **RPS** (0.40 g, yield: 58%). M.p. 211.8~213.1 °C. ^{1}H-NMR (300 MHz, $CDCl_3$): δ = 1.16 (t, J = 6.9, 12H, -CH_3), 3.32 (q, J = 6.6, 8H, -CH_2-), 6.35 (s, 4H, Ar-H), 6.85-6.87 (d, J = 8.4, 2H, Ar-H), 7.16-7.19 (m, 1H, Ar-H), 7.46-7.48 (t, J = 3.3, 2H, Ar-H), 7.98-8.06 (m, 2H, Ar-H), 8.10-8.15 (t, J = 8.1, 2H, Ar-H), 8.19-8.22 (d, J = 9, 4H, Ar-H), 8.58-8.61 (d, J = 8.1, 1H, Ar-H), 9.05-9.08 (d, J = 9.3, 1H, Ar-H), 9.58 (s, 1H, imine-H). ^{13}C-NMR (500 MHz, $CDCl_3$): 158.31, 155.49, 151.90, 148.27, 135.38, 133.08, 132.19, 131.20, 130.64, 130.32, 130.15, 128.97, 128.69, 128.44, 127.86, 127.42, 127.39, 127.17, 126.99, 126.06, 125.88, 125.75, 124.91, 124.83, 124.51, 123.57, 122.37, 110.62, 108.32, 97.57, 44.35, 12.62. Anal. Calcd for $C_{45}H_{40}N_4OS$: C, 78.92; H, 5.89; N, 8.18.

Found: C, 79.01; H, 5.94; N, 8.11. TOF-MS: m/z 685.3 $[M+H]^+$.

3. Results and discussion

Chemosensors **RPS** and **RPO** are Schiff bases and both contain a rhodamine uint and a pyrene moiety. **RPS** was synthesized by the condensation of thiooxorhodamine-B hydrazide **3** with 1-formylpyrene in 58% yield, and the reaction between rhodamine-B hydrazide **4** and 1-formylpyrene afforded **RPO** in 63% yield (Scheme 1).

<Place Figure 1 here.>

As shown in Fig. 1, the UV-vis properties of **RPS** and **RPO** were investigated towards Hg^{2+}. Without Hg^{2+}, both chemosensors showed weak absorption over 550 nm, which indicated that the spirolactam rhodamine moiety was the dominant species. Upon addition of Hg^{2+}, a new absorption band centered at 560 nm (**RPS**, $\varepsilon = 9.37\times10^4$ $L\cdot mol^{-1}\cdot cm^{-1}$; **RPO**, $\varepsilon = 6.36\times10^4$ $L\cdot mol^{-1}\cdot cm^{-1}$) appeared and the absorption coefficient increased significantly, due to the ring-opening of the rhodamine spirolactam. And the ring-opening mechanism was also responsible for the color changes from faint yellow to pink (**RPS**) and from colorless to purplish red (**RPO**), which were visually perceptible. Meanwhile, a typical pyrene absorption band appeared at 326 nm. In Fig. 1a, the absorbance of **RPS** at 326 nm and 424 nm decreased gradually, however, in Fig. 1b, the absorbance of **RPO** at 378 nm increased with the increasing amount of Hg^{2+}, which might be attributed to the influence of Hg^{2+} on the pyrene moiety. The two insets of Fig. 1 showed the absorbance at 560 nm as a function of Hg^{2+} concentrations, respectively.

<Place Figure 2 here.>

<Place Scheme 2 here.>

The fluorescence characteristics of the two chemosensors were also investigated. Before adding Hg^{2+}, free **RPS** showed a strong emission band centered at 454 nm which might be attributed to the pyrenyl excimer emission (Fig. 2a), but free **RPO** displayed no obvious emission at this wavelength (Fig. 2b). As depicted in Fig. 2a, on the gradual addition of Hg^{2+} to a solution of **RPS**, a new fluorescence emission band centered at 594 nm appeared, which was due to the ring-opening of the rhodamine spirolactam. Subsequently, the emission band changed with a blue shift in the maximum to 582 nm, which might be accounted for the intermolecular electron transfer between **RPS** and Hg^{2+}. The observed pyrenyl excimer emission at 454 nm concomitantly declined slightly, which might be a

result of Hg^{2+}-induced weak change of the stacked or folded conformation of the pyrene (Scheme 2). An isosbestic point centered at 537 nm was observed, and the fluorescence intensity ratios at I_{582}/I_{454} changed from 0.09 to 2.79, which suggested that **RPS** would be useful for quantitative determination of Hg^{2+} concentrations over a large dynamic range. This ratiometric fluorescence change also denoted that there existed a fluorescence resonance energy transfer (FRET) behavior from the pyrene excimer to rhodamine moiety. The titration curve can be used as the calibration curve for the detection of Hg^{2+}, from which the LOD and LOQ were approximately inferred as 4.34×10^{-7} mol·L^{-1} (S/N = 3) and 1.45×10^{-6} mol·L^{-1} (S/N = 10) respectively, as well as the association constant (K_a) of **RPS** with Hg^{2+} was 1.44×10^{6} M^{-1} (error < 10%).

In the case of **RPO**, remarkable changes of the fluorescence intensity at 452 nm (λ_{ex} = 365 nm) (Fig. 2b) and 576 nm (λ_{ex} = 515 nm) (Fig. 2c) were observed upon the addition of Hg^{2+}. The former change might be interpreted as the result of Hg^{2+}-induced monomer/excimer switch of the pyrene moiety. The latter change was similar to that of **RPS** at 594 nm, both resulted from the Hg^{2+}-induced ring-opening of the rhodamine spirolactam. It should be noted that there was no efficient FRET behavior observed in the **RPO** system on addition of Hg^{2+}. The insets in Fig. 2b and Fig. 2c exhibited the dependence of fluorescence intensities at 452 nm (b) and at 576 nm (c) on Hg^{2+} concentrations, respectively. From the titration results, the LOD was estimated as 1.91×10^{-5} mol·L^{-1} (S/N = 3), as well as the LOQ was 6.37×10^{-5} mol·L^{-1} (S/N = 10).

<Place Figure 3 here.>

<Place Scheme 3 here.>

The Job's plot analysis exhibited a maximum at about 0.5 mol fraction of Hg^{2+} indicating a 1:1 stoichiometry for the **RPS**/Hg^{2+} complex (Fig. 3). However, on the addition of Hg^{2+}, **RPO** was first hydrolysed to compound **5**, and then hydrolysed to rhodamine-B, which could be illustrated in Scheme 3. The proposed hydrolytic mechanism was confirmed by *ESI*-MS (Fig. S8). In the absence of Hg^{2+}, the *m/z* 669.2 peak corresponded to [**RPO**+H]$^+$ (Fig. S7), when introducing Hg^{2+} into the **RPO** ethanol aqueous solution (EtOH/H_2O, 1:1), the peak at *m/z* 669.2 disappeared, and new peaks at *m/z* 457.1 and *m/z* 443.1 appeared, which were assigned to compound **5** and rhodamine-B, respectively (Fig. S8). The hydrolysis reaction might induce the conformational changes of the resulted pyrene moiety from the weak pyrene monomer emission to strong pyrene excimer emission.

<Place Figure 4 here.>

The fluorescence spectra of **RPS** and **RPO** in the presence of several other metal cations, including K^+, Na^+, Ca^{2+}, Mg^{2+}, Cr^{3+}, Ag^+, Cu^{2+}, Co^{2+}, Ni^{2+}, Cd^{2+}, Mn^{2+}, Fe^{2+}, Zn^{2+} and Pb^{2+}, were investigated in EtOH/H_2O (1:1, v/v, pH = 7.0) (Fig. 4). While the introduction of 3 μM Hg^{2+} into **RPS** ethanol aqueous solution (3 μM) induced a remarkable change in the fluorescence intensity, the addition of other metal ions caused very weak changes, even at the mM level, such as alkali metal ions (K^+, Na^+) and alkali-earth metal ions (Ca^{2+}, Mg^{2+}). In terms of **RPO** (1 μM), the addition of various metal ions caused much weaker changes except Hg^{2+} (100 μM), which resulted in a 230-fold enhancement of fluorescence. This change is similar to that of **RPS**. Competition experiments were also conducted to corroborate a potential applicability of chemosensors **RPS** and **RPO** for the selective detection of Hg^{2+} ions in EtOH/H_2O (1:1, v/v, pH = 7.0) upon various cations. In the case of **RPO**, no significant changes were found, in addition to the solution mixed with Mn^{2+}, which reduced the fluorescence intensity. Nevertheless, these results indicated that the competed ions would not interfere with the recognition of Hg^{2+} by **RPS** and **RPO**, thus it was demonstrated that both **RPS** and **RPO** could be served as potential Hg^{2+}-selective chemosensors.

<Place Figure 5 here.>

To examine the reversibility of the proposed **RPS**/Hg^{2+} species and **RPO**/Hg^{2+} species, Na_2S-addition experiments were conducted. The addition of 0.3 mL Na_2S restored the initial value of free **RPS** since the K_d value of $[HgS_2]^{2-}$ was 10^{-50} M^2, which was much higher than K_a [**RPS**/Hg^{2+}] [14], and the initial color pink faded (Fig. 5a). However, when **RPO** interacted with Hg^{2+} completely, the addition of excess Na_2S made no changes of the solution, neither in the fluorescence intensity nor in the color change (Fig. 5b and Fig. 5c). The irreversibility of **RPO**/Hg^{2+} corroborated the hydrolytic mechanism of **RPO** with Hg^{2+}.

<Place Figure 6 here.>

In addition, for practical applications, the effect of pH on the fluorescence emission of **RPS** and **RPO** in the absence and presence of Hg^{2+} with different pH conditions in EtOH/H_2O (1:1, v/v) was also explored (Fig. 6). The solution of **RPS** exhibited very weak fluorescence and elicited negligible changes between pH 5.5 and 12.0. Compared with free **RPO**, the fluorescence intensity increased dramatically in the pH range of 3.0 ~ 9.0 when interacted with Hg^{2+}. Between pH 6.5 and 9.0, the intensity was relatively stable, but decreased at pH > 9.0 (Fig. 6a). The solution of free **RPO** displayed almost no fluorescence with the change of pH value, whereas, it exhibited apparent

fluorescence emission in the presence of Hg^{2+}, and the fluorescence intensity enhanced slightly with the increase of pH value, but changed little between 6.5 and 8.0 (Fig. 6b). All these results demonstrated that both chemosensor **RPS** and **RPO** could be applied in recognizing Hg^{2+} under near neutral pH conditions.

<Place Figure 7 here.>

The **RPS** sensor exhibited a rapid fluorescence response to Hg^{2+}. All the tests of **RPS** with Hg^{2+} were conducted in 5 min after the addition of Hg^{2+}. Nevertheless, the response of **RPO** to Hg^{2+} was not as quick as that of **RPS** to Hg^{2+}. The time dependence of the fluorescence of **RPO** was illustrated in Fig. 7. The fluorescence intensity of **RPO** with Hg^{2+} leveled off after about 80 min, which was much slower than that of **RPS**. For practical application, chemosensor **RPS** was also employed to detect Hg^{2+} by doping tap water with Hg^{2+} (Table 1).

<Place Table 1 here.>

Keeping all the aforementioned results in mind, we would find that chemosensor **RPS** is superior to **RPO** with the following considerations: (i) the detection limit of **RPS** (4.34×10^{-7} mol·L^{-1}) is much lower than that of **RPO** (1.91×10^{-5} mol·L^{-1}); (ii) the response time of **RPS** to Hg^{2+} is much shorter than that of **RPO**; (iii) the reversibility of **RPS**/Hg^{2+} has an advantage over **RPO**/Hg^{2+}; (iv) a FRET behavior was observed in the combination of **RPS** with Hg^{2+}, which could not be obtained in the combination of **RPO** with Hg^{2+}; (v) upon the interaction with Hg^{2+}, **RPS** showed a 1:1 stoichiometry for the **RPS**/Hg^{2+} complex, however, **RPO** was hydrolyzed; (vi) chemosensor **RPS** can be well applied in the water sample for the detection of Hg^{2+}.

4. Conclusion

In summary, two novel rhodamine-pyrene derivatives **RPS** and **RPO** have been successfully designed as ratiometric chromogenic and fluorogenic chemosensors for sensitive, selective, and reversible detection of Hg^{2+} in aqueous medium. The significant color changes could be used for direct visual detection. The stoichiometry of the **RPS**/Hg^{2+} complex is 1:1. The FRET efficiency changed during the combination of **RPS** with Hg^{2+}, whereas, a hydrolytic reaction occurred when adding Hg^{2+} into the ethanol aqueous solution of **RPO**. To detect Hg^{2+}, **RPS** is superior to **RPO** for its lower detection limit, shorter response time and advantageous reversibility, presumably due to the thiophilic nature of mercury and the different sensing mechanisms in operation. And **RPS** can be well

applied in the water sample for the detection of Hg^{2+}.

Acknowledgments

This work is supported by the Open Fund of the State Key Laboratory of Materials-Oriented Chemical Engineering, the postgraduate practice innovation fund of Jiangsu province (CXZZ12-0444), and the doctor thesis innovation fund of Nanjing University of Technology.

References

[1] (a) Boening DW. Ecological effects, transport, and fate of mercury: a general review. Chemosphere 2000; 40: 1335-51.

(b) Harris HH, Pickering IJ, George GN. The Chemical Form of Mercury in Fish. Science 2003; 301(5637): 1203.

[2] (a) Wang F, Nam SW, Guo ZQ, Park S, Yoon J. A new rhodamine derivative bearing benzothiazole and thiocarbonyl moieties as a highly selective fluorescent and colorimetric chemodosimeter for Hg^{2+}. Sensor Actuat B 2012; 161: 948-53.

(b) Chen XQ, Pradhan T, Wang F, Kim JS, Yoon J. Fluorescent Chemosensors Based on Spiroring-Opening of Xanthenes and Related Derivatives. Chem Rev 2012; 112: 1910-56.

(c) Renzoni A, Zino F, Franchi E. Mercury Levels along the Food Chain and Risk for Exposed Populations. Environ Res 1998; 77(2): 68-72.

(d) Benoit JM, Fitzgerald WF, Damman AWH. The Biogeochemistry of an Ombrotrophic Bog: Evaluation of Use as an Archive of Atmospheric Mercury Deposition. Environ Res 1998; 78(2): 118-33.

[3] Liu K, Zhou Y, Yao C. A highly sensitive and selective ratiometric and colorimetric sensor for Hg^{2+} based on a rhodamine–nitrobenzoxadiazole conjugate. Inorg Chem Commun 2011; 14: 1798-801.

[4] (a) Ling LX, Zhao Y, Du J, Xiao D. An optical sensor for mercuric ion based on immobilization of Rhodamine B derivative in PVC membrane. Talanta 2012; 91: 65-71.

(b) Ugo P, Moretto LM, Bertoncello P, Wang J. Determination of Trace Mercury in Saltwaters at Screen-Printed Electrodes Modified with Sumichelate Q10R. Electroanalysis 1998; 10(15): 1017-21.

(c) Capelo JL, Lavilla I, Bendicho C. Room Temperature Sonolysis-Based Advanced Oxidation Process for Degradation of Organomercurials: Application to Determination of Inorganic and Total Mercury in Waters by Flow Injection-Cold Vapor Atomic Absorption Spectrometry. Anal Chem 2000; 72: 4979-84.

(d) Koulouridakis PE, Kallithrakas-Kontos NG. Selective Mercury Determination after Membrane Complexation and Total Reflection X-ray Fluorescence Analysis. Anal Chem 2004; 76(15): 4315-9.

(e) Gómez-Ariza JL, Lorenzo F, García-Barrera T. Comparative study of atomic fluorescence

spectroscopy and inductively coupled plasma mass spectrometry for mercury and arsenic multispeciation. Anal Bioanal Chem 2005; 382(2): 485-92.

(f) Han FX, Patterson WD, Xia YJ, Sridhar BBM, Su Y. Rapid Determination of Mercury in Plant and Soil Samples Using Inductively Coupled Plasma Atomic Emission Spectroscopy, a Comparative Study. Water Air Soil Pollut 2006; 170(1-4): 161-71.

(g) Fong MW, Siu TS, Lee SK, Tam S. Determination of Mercury in Whole Blood and Urine by Inductively Coupled Plasma Mass Spectrometry. J Anal Toxicol 2007; 31(5): 281-7.

(h) Geng WH, Nakajima T, Takanashi H, Ohki A. Determination of mercury in ash and soil samples by oxygen flask combustion method–Cold vapor atomic fluorescence spectrometry (CVAFS). J Hazard Mater 2008; 154(1-3): 325-30.

(i) Yu YL, Du Z, Wang JH. The development of a miniature atomic fluorescence spectrometric system in a lab-on-valve for mercury determination. J Anal At Spectrom 2007; 22: 650-6.

(j) Yu X, Zhou ZD, Wang Y, Liu Y, Xie Q, Xiao D. Mercury(II)-selective polymeric membrane electrode based on the 3-[4-(dimethylamino)phenyl]-5-mercapto-1,5-diphenylpentanone. Sens Actuators B 2007; 123(1): 352-8.

(k) Bühlmann P, Pretsch E, Bakker E. Carrier-Based Ion-Selective Electrodes and Bulk Optodes. 2. Ionophores for Potentiometric and Optical Sensors. Chem Rev 1998; 98(4): 1593-688.

[5] (a) Zhou Y, You XY, Fang Y, Li JY, Liu K, Yao C. A thiophen-thiooxorhodamine conjugate fluorescent probe for detecting mercury in aqueous media and living cells. Org Biomol Chem 2010; 8: 4819-22.

(b) Lakowicz JR. Principles of fluorescence spectroscopy. 3rd ed. New York: Springer; 2006.

[6] Bag B, Pal A. Rhodamine-based probes for metal ion-induced chromo-/fluorogenic dual signaling and their selectivity towards Hg(II) ion. Org Biomol Chem 2011; 9: 4467-80.

[7] Quang DT, Wu JS, Luyen ND, Duong T, Dan ND, Bao NC, Quy PT. Rhodamine-derived Schiff base for the selective determination of mercuric ions in water media. Spectrochimica Acta Part A 2011; 78(2): 753-6.

[8] (a) Zheng H, Qian ZH, Xu L, Yuan FF, Lan LD, Xu JG. Switching the Recognition Preference of Rhodamine B Spirolactam by Replacing One Atom: Design of Rhodamine B Thiohydrazide for Recognition of Hg(II) in Aqueous Solution. Org Lett 2006; 8(5): 859-61.

(b) Lee MH, Wu JS, Lee JW, Jung JH, Kim JS. Highly Sensitive and Selective Chemosensor for Hg^{2+} Based on the Rhodamine Fluorophore. Org Lett 2007; 9(13): 2501-4.

(c) Yang H, Zhou ZG, Huang KW, Yu MX, Li FY, Yi T, Huang CH. Multisignaling Optical-Electrochemical Sensor for Hg^{2+} Based on a Rhodamine Derivative with a Ferrocene Unit. Org Lett 2007; 9(23): 4729-32.

(d) Wu DY, Huang W, Duan CY, Lin ZH, Meng QJ. Highly Sensitive Fluorescent Probe for Selective Detection of Hg^{2+} in DMF Aqueous Media. Inorg Chem 2007; 46(5): 1538-40.

(e) Shiraishi Y, Sumiya S, Kohno Y, Hirai T. A Rhodamine−Cyclen Conjugate as a Highly Sensitive and Selective Fluorescent Chemosensor for Hg(II). J Org Chem 2008; 73(21): 8571-4.

(f) Suresh M, Mishra S, Mishra SK, Suresh E, Mandal AK, Shrivastav A, Das A. Resonance Energy Transfer Approach and a New Ratiometric Probe for Hg^{2+} in Aqueous Media and Living Organism. Org Lett 2009; 11(13): 2740-3.

(g) Huang JH, Xu YF, Qian XH. A Rhodamine-Based Hg^{2+} Sensor with High Selectivity and Sensitivity in Aqueous Solution: A NS_2-Containing Receptor. J Org Chem 2009; 74(5): 2167-70.

(h) Lee MH, Giap TV, Kim SH, Lee YH, Kang C, Kim JS. A novel strategy to selectively detect Fe(III) in aqueous media driven by hydrolysis of a rhodamine 6G Schiff base. Chem Commun 2010; 46: 1407-9.

[9] (a) Zhou Y, Zhu CY, Gao XS, You XY, Yao C. Hg^{2+}-Selective Ratiometric and "Off-On" Chemosensor Based on the Azadiene-Pyrene Derivative. Org Lett 2010; 12(11): 2566-9.

(b) Park SM, Kim MH, Choe JI, Tai No KT, Chang SK. Cyclams Bearing Diametrically Disubstituted Pyrenes as Cu^{2+}- and Hg^{2+}-Selective Fluoroionophores. J Org Chem 2007; 72(9): 3550-3.

[10] (a) Kim JS, Choi MG, Song KC, No KT, Ahn S, Chang SK. Ratiometric Determination of Hg^{2+} Ions Based on Simple Molecular Motifs of Pyrene and Dioxaoctanediamide. Org Lett 2007; 9(6): 1129-32.

(b) Shiraishi Y, Tokitoh Y, Hirai T. pH- and H_2O-Driven Triple-Mode Pyrene Fluorescence. Org Lett 2006; 8(17): 3841-4.

(c) Yuasa H, Miyagawa N, Izumi T, Nakatani M, Izumi M, Hashimoto H. Hinge Sugar as a Movable Component of an Excimer Fluorescence Sensor. Org Lett 2004; 6(9): 1489-92.

(d) Kim JS, Noh KH, Lee SH, Kim SK, Kim SK, Yoon J. Molecular Taekwondo. 2. A New

Calix[4]azacrown Bearing Two Different Binding Sites as a New Fluorescent Ionophore. J Org Chem 2003; 68(2): 597-600.

(e) Winnik FM. Photophysics of preassociated pyrenes in aqueous polymer solutions and in other organized media. Chem Rev 1993; 93(2): 587-614.

(f) Choi JK, Kim SH, Yoon J, Lee KH, Bartsch RA, Kim JS. A PCT-Based, Pyrene-Armed Calix[4]crown Fluoroionophore. J Org Chem 2006; 71(21): 8011-5.

(g) Moon SY, Youn NJ, Park SM, Chang SK. Diametrically Disubstituted Cyclam Derivative Having Hg^{2+}-Selective Fluoroionophoric Behaviors. J Org Chem 2005; 70(6): 2394-7.

(h) Xie J, Ménand M, Maisonneuve S, Métivier R. Synthesis of Bispyrenyl Sugar-Aza-Crown Ethers as New Fluorescent Molecular Sensors for Cu(II). J Org Chem 2007; 72: 5980-5.

(i) Hung HC, Cheng CW, Ho IT, Chung WS. Dual-mode recognition of transition metal ions by bis-triazoles chained pyrenes. Tetrahedron Lett 2009; 50: 302-5.

[11] Zhou Y, Wang F, Kim Y, Kim SJ, Yoon J. Cu^{2+}-Selective Ratiometric and "Off-On" Sensor Based on the Rhodamine Derivative Bearing Pyrene Group. Org Lett 2009; 11(19): 4442-5.

[12] (a) Lee YH, Lee MH, Zhang JF, Kim JS. Pyrene Excimer-Based Calix[4]arene FRET Chemosensor for Mercury(II). J Org Chem 2010; 75(21): 7159-65.

(b) Kim HN, Ren WX, Kim JS, Yoon J. Fluorescent and colorimetric sensors for detection of lead, cadmium, and mercury ions. Chem Soc Rev 2012; 41: 3210-44.

[13] Xiang Y, Tong AJ, Jin PY, Ju Y. New Fluorescent Rhodamine Hydrazone Chemosensor for Cu(II) with High Selectivity and Sensitivity. Org Lett 2006; 8(13): 2863-6.

[14] (a) Armstrong RD, Porter DF, Thirsk HR. Passivation of mercury in sulfide ion solutions. J Phys Chem 1968; 72(7): 2300-6.

(b) Findlay DM, McLean RAN. Removal of elemental mercury from wastewaters using polysulfides. Environ Sci Technol 1981; 15(11): 1388-90.

Figure captions

Figure 1. (a) UV-vis spectra of **RPS** (3 μM) in the presence of different concentrations of Hg^{2+} (0-4 μM) in EtOH/H_2O (1:1, v/v, pH = 7.0). (b) UV-vis spectra of **RPO** (5 μM) in the presence of different concentrations of Hg^{2+} (0-500 μM) in EtOH/H_2O (1:1, v/v, pH = 7.0). Insets: the absorbance at 560 nm as a function of Hg^{2+} concentrations.

Figure 2. (a) Fluorescence titration of **RPS** (3 μM) in EtOH/H_2O (1:1, v/v, pH = 7.0) in the presence of different concentrations of Hg^{2+} (0-4 μM). Inset: the ratio of fluorescence intensity at 582 nm and 454 nm as a function of Hg^{2+} concentrations. Excitation wavelength was 365 nm. (b) and (c) Fluorescence titration of **RPO** (1 μM) in EtOH/H_2O (1:1, v/v, pH = 7.0) in the presence of different concentrations of Hg^{2+} (0-300 μM). (b) The fluorescence spectra of **RPO** with the fluorescence enhancement at 452 nm upon the excitation at 365 nm. Inset: fluorescence intensity at 452 nm as a function of Hg^{2+} concentrations. (c) The fluorescence spectra of **RPO** with the fluorescence enhancement at 576 nm upon the excitation at 515 nm. Inset: fluorescence intensity at 576 nm as a function of Hg^{2+} concentrations.

Figure 3. The Job's plot of chemosensor **RPS**, with a total concerntration of ([RPS] + [Hg^{2+}]) = 10 μM. The detection wavelength was 560 nm.

Figure 4. (a) Fluorescence responses of 3 μM **RPS** to various 10 μM transition metal ions (1 mM for alkali and alkali-earth metal ions). Spectra were acquired in EtOH/H_2O (1:1, v/v, pH = 7.0). Bars represent the ratio of fluorescence intensity at 582 nm (F_{582}) over that at 454 nm (F_{454}). The black bars represent the fluorescence emission of 3 μM **RPS** solution with different competing metal ions. The red bars represent the change of the emission that occurs on the subsequent addition of 3 μM Hg^{2+} to the above solutions. (b) Fluorescence responses of 1 μM **RPO** to various 10 μM transition metal ions (1 mM for alkali and alkali-earth metal ions). Spectra were acquired in EtOH/H_2O (1:1, v/v, pH = 7.0). Bars represent the final (F_f) over the initial (F_i) integrated emission. The black bars represent the fluorescence emission of 1 μM **RPO** solution with different competing metal ions. The red bars represent the change of the emission that occurs on the subsequent addition of 100 μM Hg^{2+} to the above solution.

Figure 5. (a) Reversibility of Hg^{2+} to **RPS** by Na_2S. Red line: free **RPS** (3 μM), blue line: **RPS** + 1

equiv of Hg^{2+}, black line: **RPS** + 1 equiv of Hg^{2+} + 0.3 mL of Na_2S (0.1 mM). (b) and (c) Reversibility of Hg^{2+} to **RPO** by Na_2S. Red line: free **RPO** (1 μM), blue line: **RPO** + 100 equiv of Hg^{2+}, black line: **RPO** + 100 equiv of Hg^{2+} + 0.6 mL of Na_2S (0.1 mM). (b) The change of fluorescence intensity at 452 nm, λ_{ex} = 365 nm. (c) The change of fluorescence intensity at 576 nm, λ_{ex} = 515 nm.

Figure 6. (a) Fluorescence intensity (582 nm) of **RPS** (3 μM) in the absence (red line) and presence (black line) of 1 equiv Hg^{2+} in EtOH/H_2O (1:1, v/v) at different pH**.** (b) Fluorescence intensity (576 nm) of **RPO** (1 μM) in the absence (red line) and presence (black line) of 100 equiv Hg^{2+} in EtOH/H_2O (1:1, v/v) at different pH**.**

Figure 7. Time dependence of the fluorescence of **RPO** with Hg^{2+} in EtOH/H_2O (1:1, v/v, pH = 7.0).

Scheme 1. Synthesis of **RPS** and **RPO**

Scheme 2. Proposed mechanism of **RPS** with Hg^{2+}.

Scheme 3. Proposed hydrolytic mechanism of **RPO** with the addition of Hg^{2+}.

Table 1. Determination of the concentrations of Hg^{2+} in water samples by fluorescent method using **RPS**.

Table 1. Determination of the concentrations of Hg^{2+} in water samples by fluorescent method using **RPS**.

Addition of Hg^{2+} /10^{-6} M	I_{582nm} / I_{454nm}	Measured value of Hg^{2+} /10^{-6} M	Recovery
2.4	1.241	2.32	96.67%
3.2	2.473	3.06	95.62%

Figure 1.tif
Click here to download high resolution image

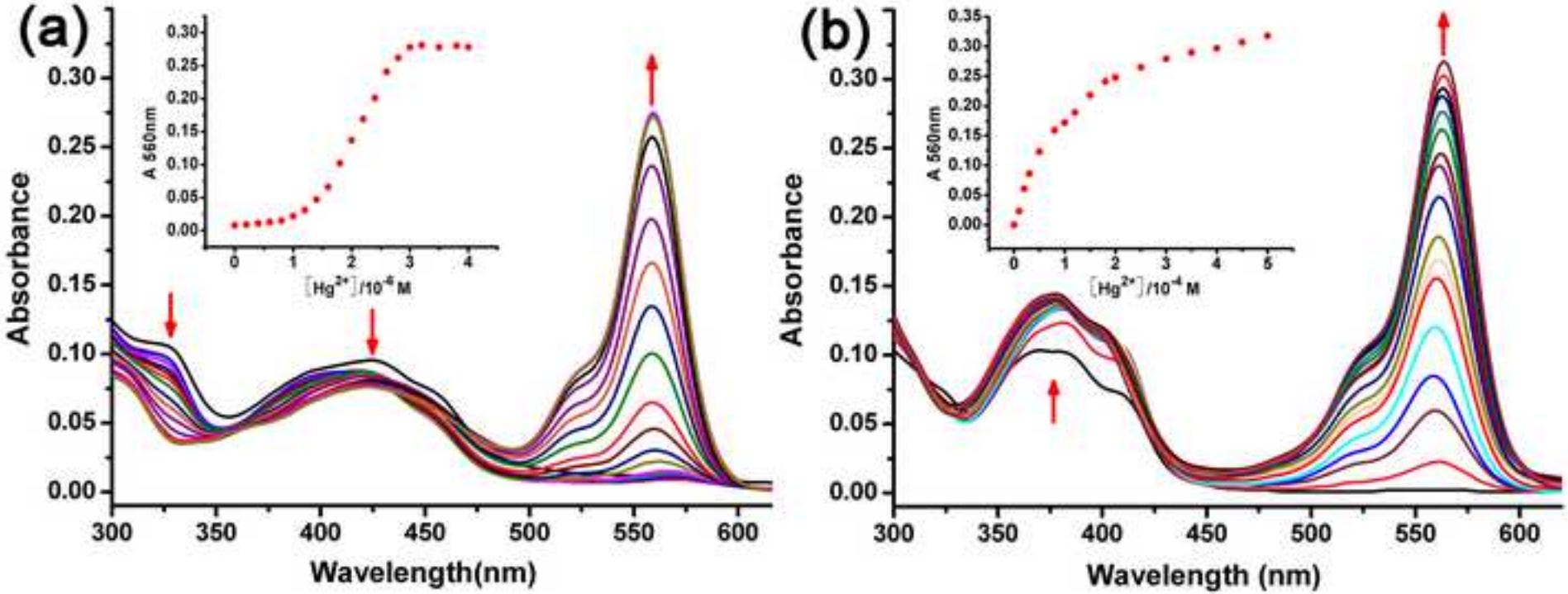

Figure 2.tif
Click here to download high resolution image

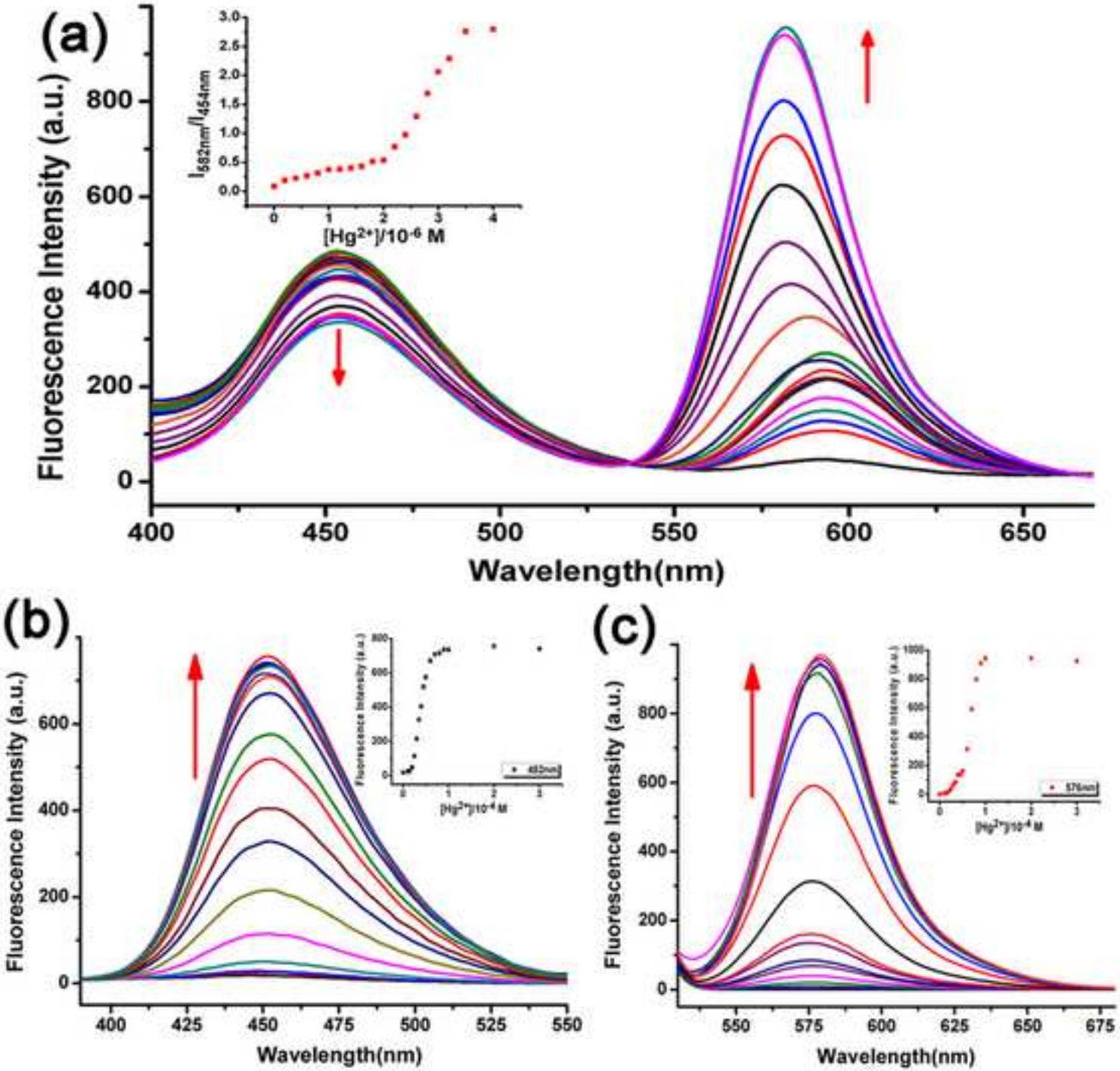

Figure 3.tif
Click here to download high resolution image

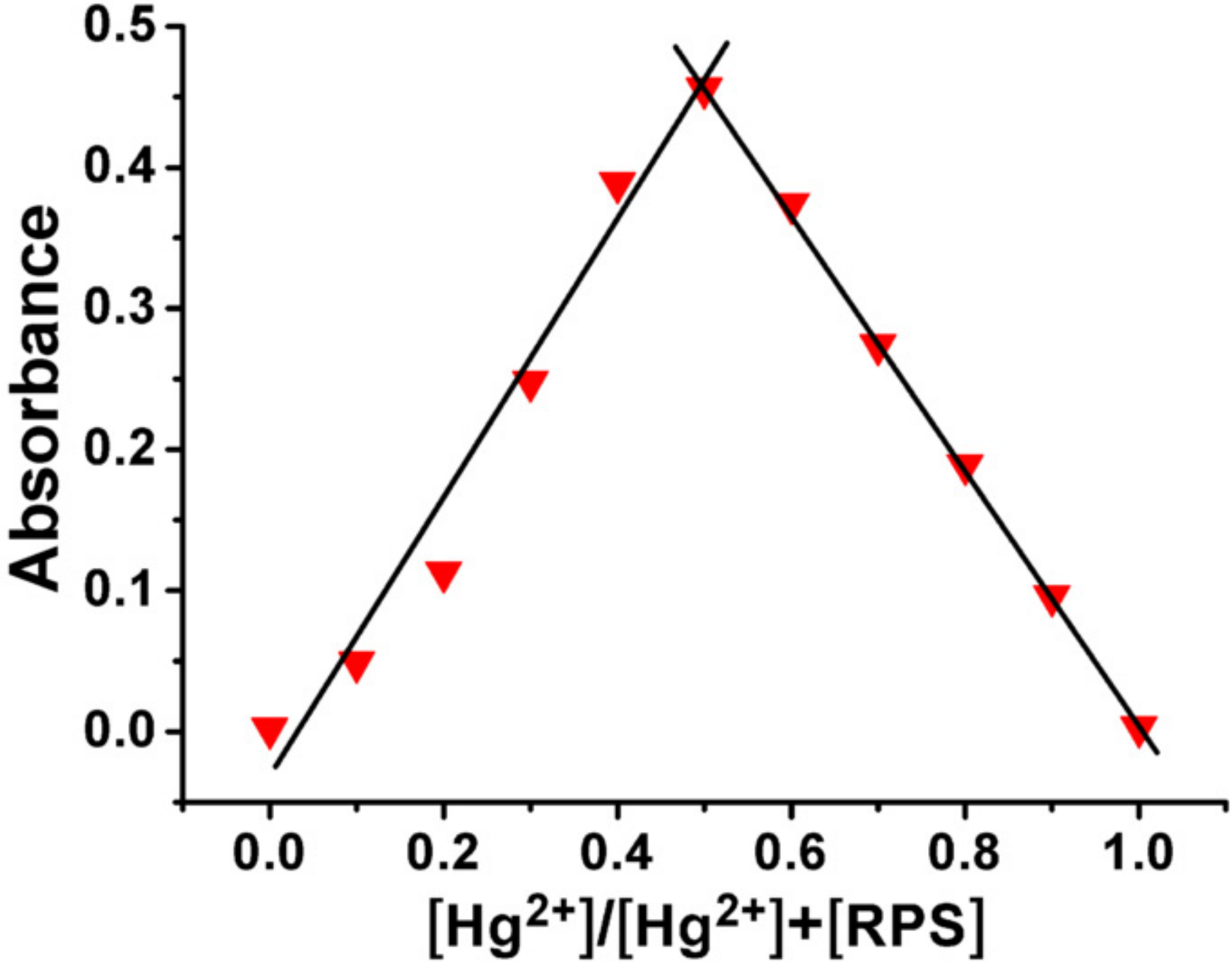

Figure 4.tif
Click here to download high resolution image

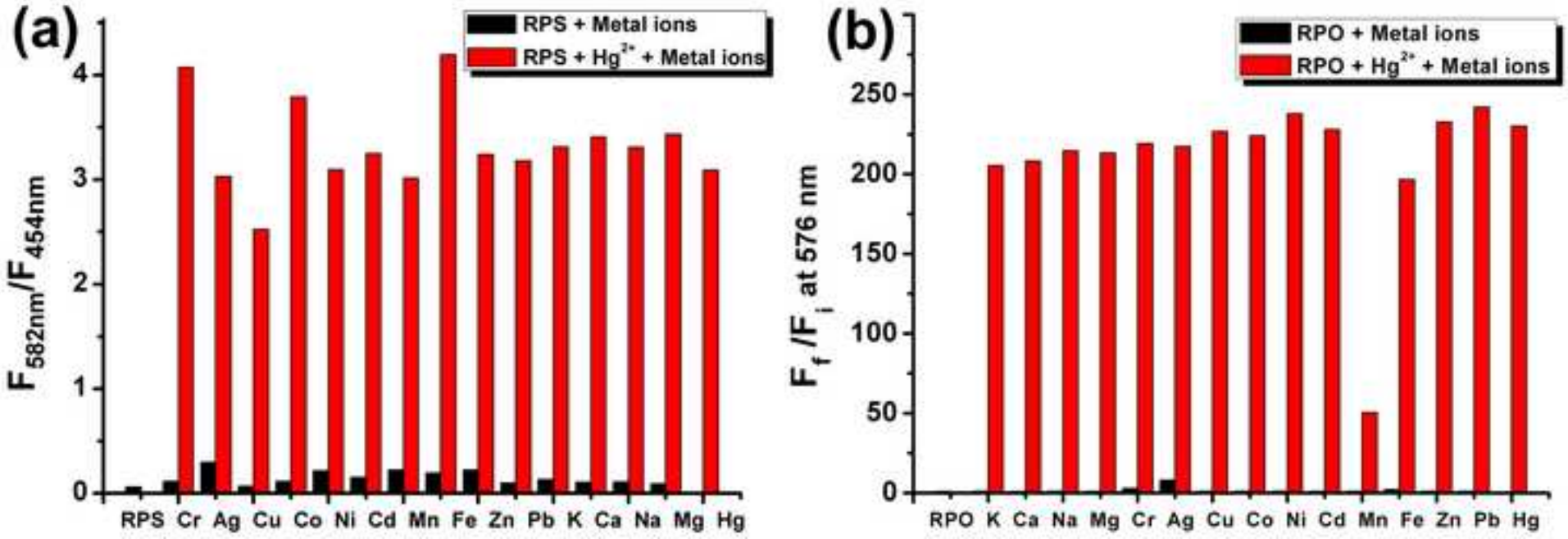

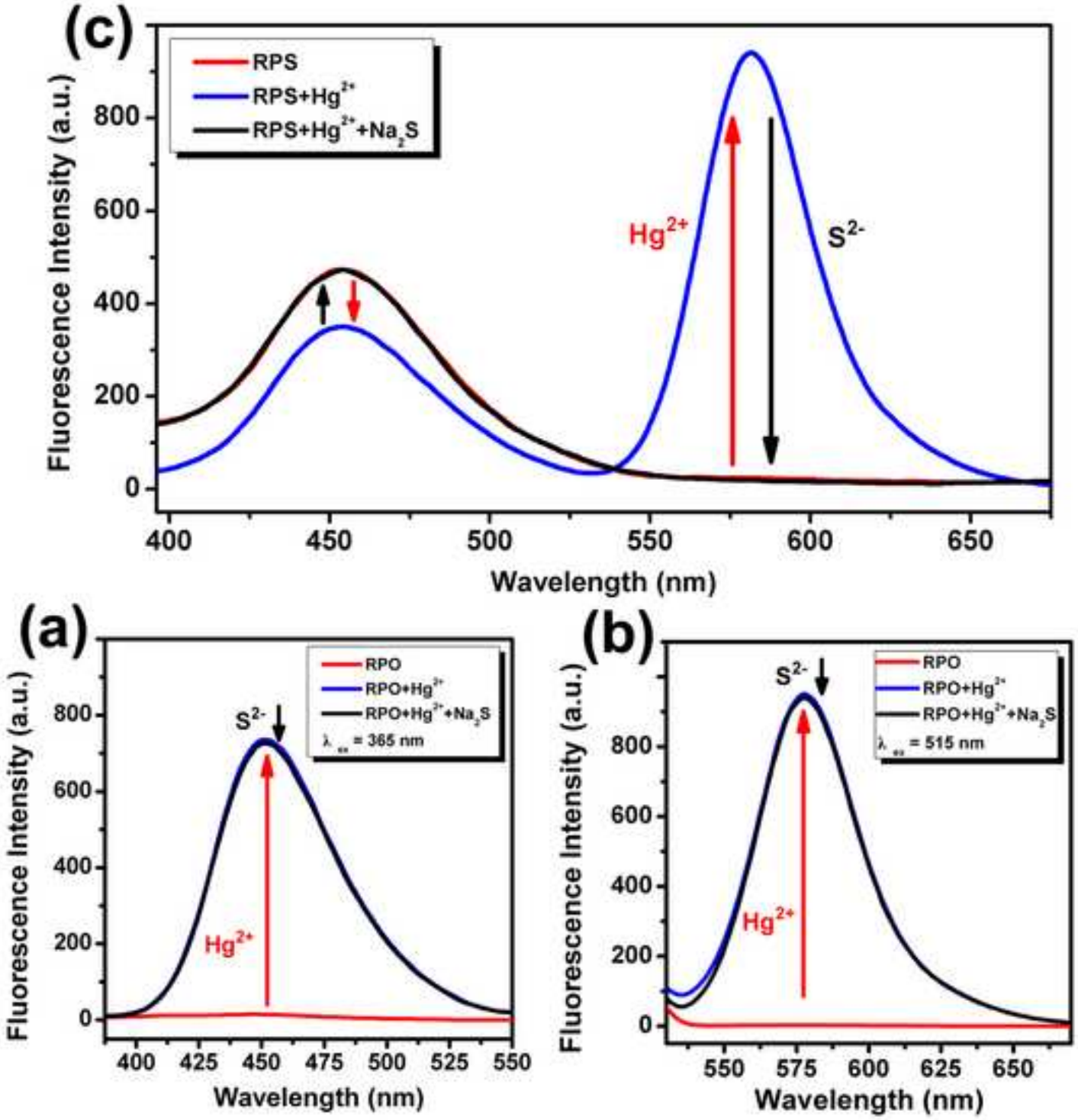

Figure 6.tif
Click here to download high resolution image

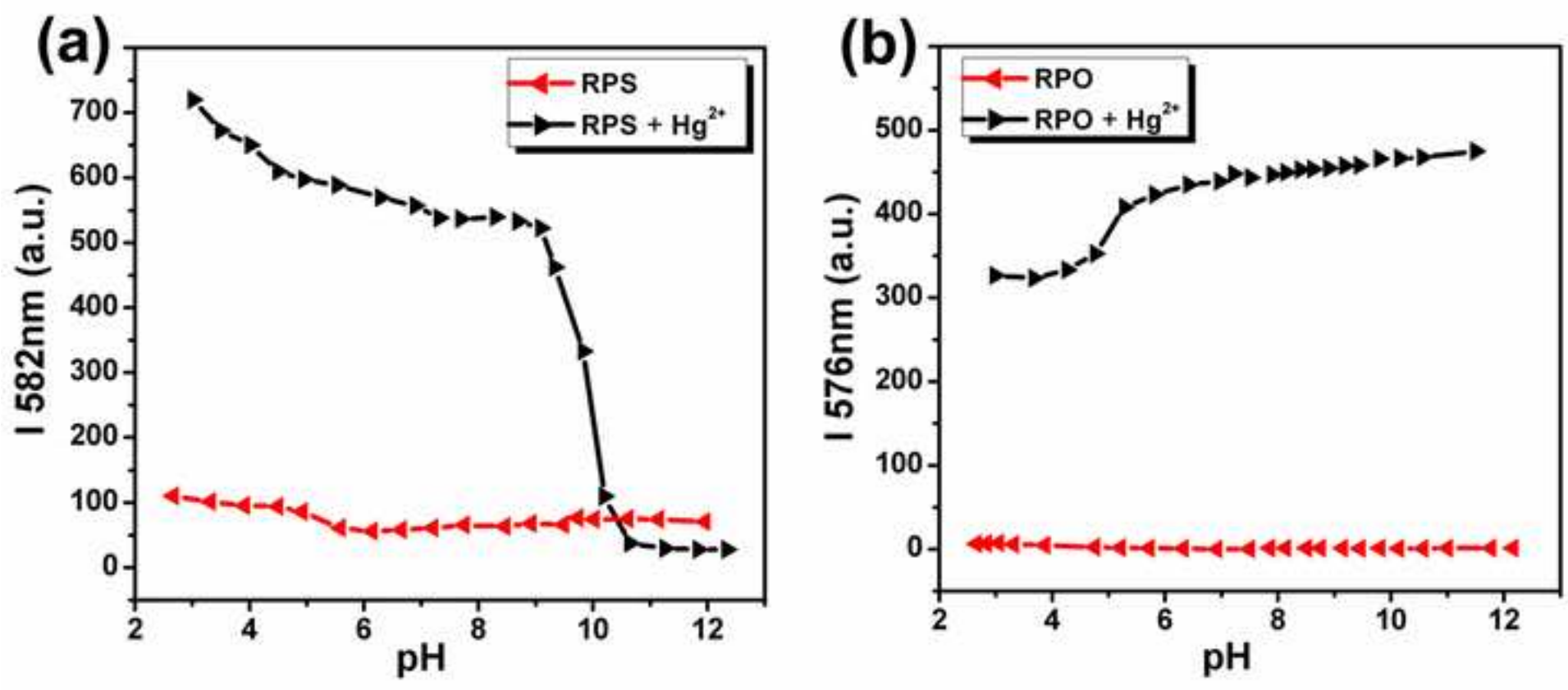

Figure 7.tif
Click here to download high resolution image

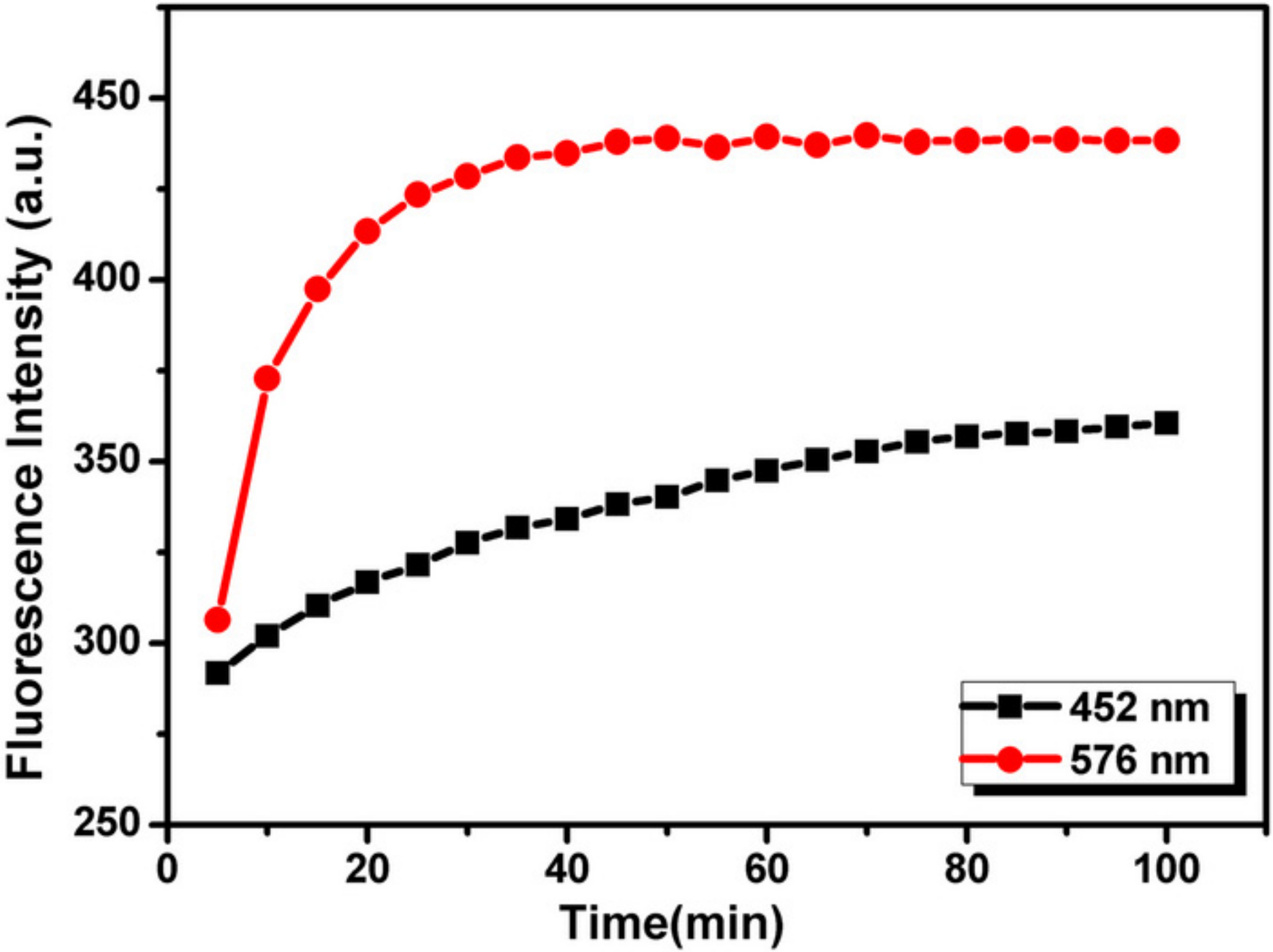

Scheme 1.tif

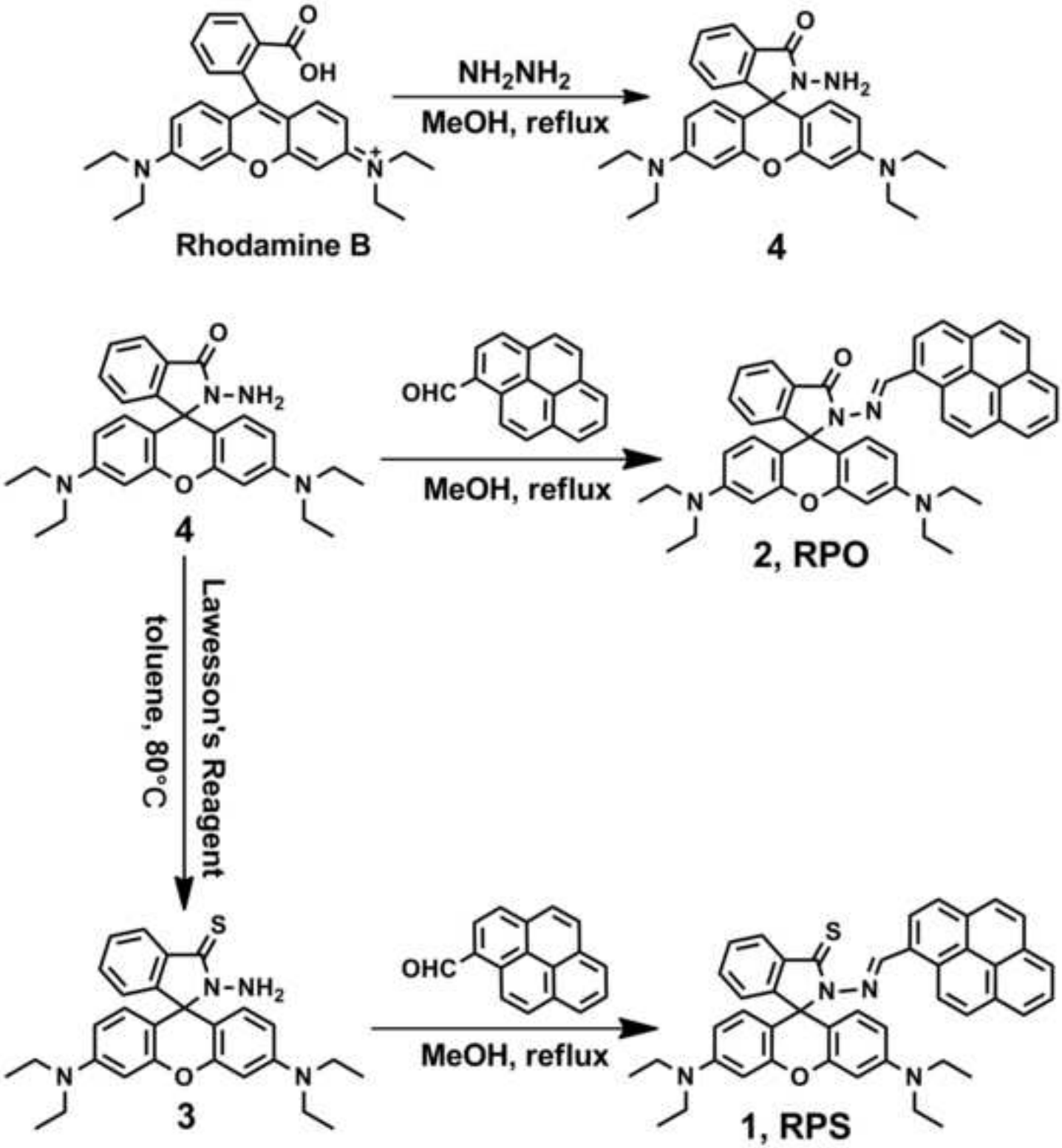

Scheme 2.TIF
Click here to download high resolution image

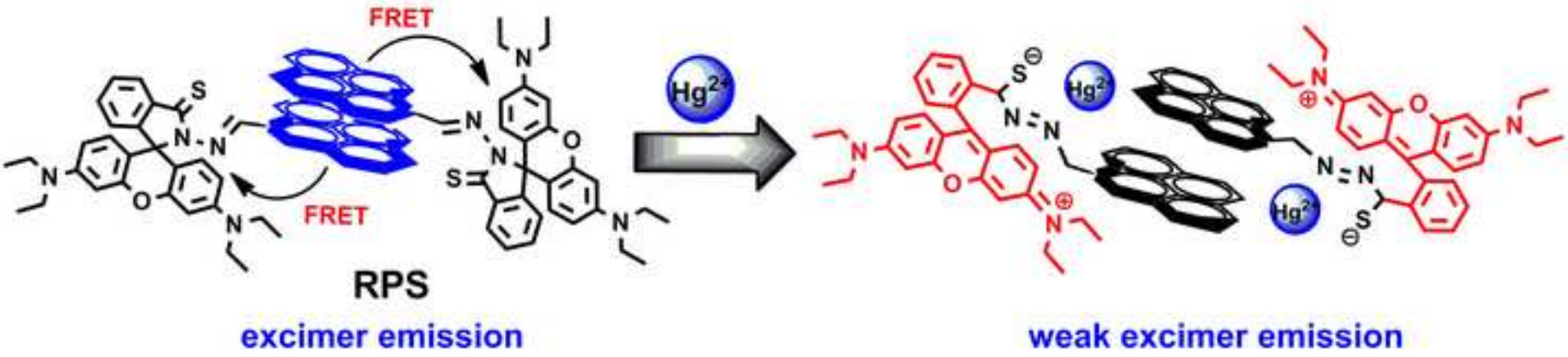

Scheme 3.TIF
Click here to download high resolution image

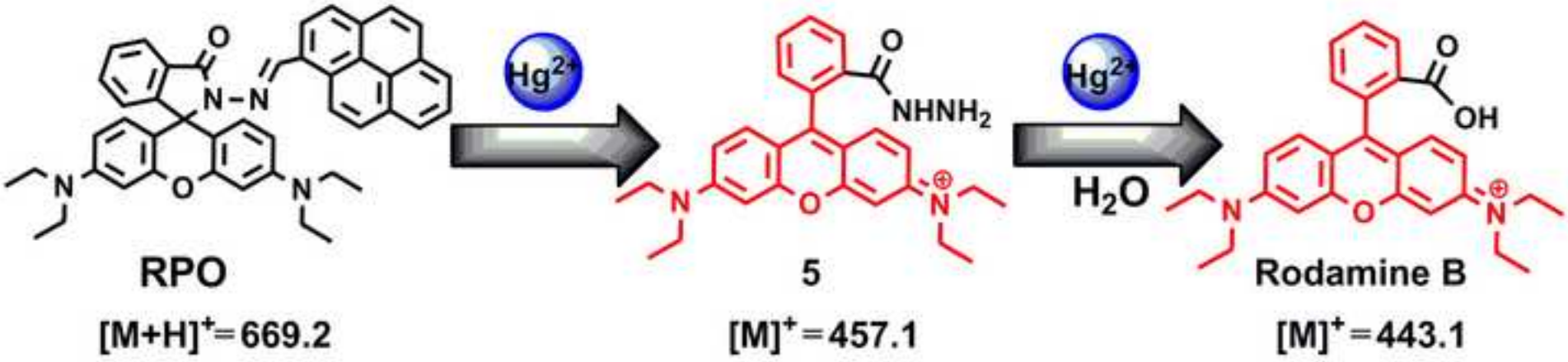

Highlights

- Two chemosensors, differentiated by a spirothiolactone and a spirolactone unit, based on a rhodamine-pyrene platform were synthesized.
- With the addition of Hg^{2+}, the spirothiolactone sensor exhibited a weakened FRET behavior, while the spirolactone chemosensor was hydrolyzed inducing a large monomer-excimer switch.
- Both chemosensors exhibited colorimetric and fluorescent dual-responses towards Hg^{2+}.
- Both chemosensors could be used for ratiometric detection of Hg^{2+}.